Since January 2020 Elsevier has created a COVID-19 resource centre with free information in English and Mandarin on the novel coronavirus COVID-19. The COVID-19 resource centre is hosted on Elsevier Connect, the company's public news and information website.

European Journal of Pharmaceutical Sciences 155 (2020) 105537

Contents lists available at ScienceDirect

European Journal of Pharmaceutical Sciences

journal homepage: www.elsevier.com/locate/ejps

Discovery of HIV entry inhibitors via a hybrid CXCR4 and CCR5 receptor pharmacophore-based virtual screening approach

Muhammad Usman Mirza[a], Atefeh Saadabadi[b,c], Michiel Vanmeert[a], Outi M.H. Salo-Ahen[b,c], Iskandar Abdullah[d], Sandra Claes[e], Steven De Jonghe[e], Dominique Schols[e], Sarfraz Ahmad[d], Matheus Froeyen[a,*]

[a] Medicinal Chemistry, Department of Pharmaceutical and Pharmacological Sciences, Rega Institute for Medical Research, KU Leuven, B-3000 Leuven, Belgium
[b] Pharmaceutical Sciences Laboratory, Faculty of Science and Engineering, Pharmacy, Åbo Akademi University, FI-20520 Turku, Finland
[c] Structural Bioinformatics Laboratory, Faculty of Science and Engineering, Biochemistry, Åbo Akademi University, FI-20520 Turku, Finland
[d] Department of Chemistry, Faculty of Sciences, University Malaya, Kuala Lumpur 59100, Malaysia
[e] Laboratory of Virology and Chemotherapy, Department of Microbiology, Immunology and Transplantation, Rega Institute for Medical Research, KU Leuven, B-3000 Leuven, Belgium

ARTICLE INFO

Keywords:
HIV-1
Virtual screening
Chemokine receptors
CCR5
CXCR4

ABSTRACT

Chemokine receptors are key regulators of cell migration in terms of immunity and inflammation. Among these, CCR5 and CXCR4 play pivotal roles in cancer metastasis and HIV-1 transmission and infection. They act as essential co-receptors for HIV and furnish a route to the cell entry. In particular, inhibition of either CCR5 or CXCR4 leads very often the virus to shift to a more virulent dual-tropic strain. Therefore, dual receptor inhibition might improve the therapeutic strategies against HIV. In this study, we aimed to discover selective CCR5, CXCR4, and dual CCR5/CXCR4 antagonists using both receptor- and ligand-based computational methods. We employed this approach to fully incorporate the interaction attributes of the binding pocket together with molecular dynamics (MD) simulations and binding free energy calculations. The best hits were evaluated for their anti-HIV-1 activity against CXCR4- and CCR5-specific NL4.3 and BaL strains. Moreover, the Ca^{2+} mobilization assay was used to evaluate their antagonistic activity. From the 27 tested compounds, three were identified as inhibitors: compounds **27** (CCR5), **6** (CXCR4) and **3** (dual) with IC_{50} values ranging from 10.64 to 64.56 μM. The binding mode analysis suggests that the active compounds form a salt bridge with the glutamates and π-stacking interactions with the aromatic side chains binding site residues of the respective co-receptor. The presented hierarchical virtual screening approach provides essential aspects in identifying potential antagonists in terms of selectivity against a specific co-receptor. The compounds having multiple heterocyclic nitrogen atoms proved to be relatively more specific towards CXCR4 inhibition as compared to CCR5. The identified compounds serve as a starting point for further development of HIV entry inhibitors through synthesis and quantitative structure-activity relationship studies.

1. Introduction

The most effective treatment of patients infected with human immunodeficiency virus 1 (HIV-1) is currently highly active antiretroviral therapy (HAART), which utilizes a combination of several drugs targeting viral proteins such as reverse transcriptase, integrase and protease (Cobucci et al., 2015, Oliva-Moreno and Trapero-Bertran, 2018). An alternative approach relies on the multi-targeted inhibition of viral cell entry (Grande et al., 2019), which consists of a series of structural events arbitrated by viral and cellular membrane proteins. The interaction between the HIV-1 glycoprotein gp120 and the cellular receptor CD4 is an important initial step in viral entry. It induces a conformational change in gp120 and mediates further interaction with either one of the two co-receptors, chemokine receptor 5 (CCR5) and CXC-chemokine receptor 4 (CXCR4) during viral entry into the host cells (Shepherd et al., 2013, Chen, 2019). Both chemokine receptors belong to the G-protein coupled receptor family and regulate HIV-1 cellular tropism. CCR5-tropic or R5 strains preferentially uses CCR5, whereas CXCR4-tropic or X4 strains preferentially use CXCR4. Dual-tropic strains use both co-receptors for their entry in the $CD4^+$ target cells (Chen, 2019, Dragic et al., 1996, Scarlatti et al., 1997).

* Corresponding author.
E-mail address: matheus.froeyen@kuleuven.be (M. Froeyen).

https://doi.org/10.1016/j.ejps.2020.105537
Received 1 July 2020; Received in revised form 10 August 2020; Accepted 30 August 2020
Available online 02 September 2020

The chemokine ligand 5 (CCL5) also known as RANTES (regulated upon activation, normal T cell expressed, and secreted) is the natural ligand for CCR5 (Chien et al., 2018), whereas the CXC-chemokine ligand 12 (CXCL12), also known as SDF-1 (stromal cell-derived factor 1) is the natural ligand for CXCR4 (Smith et al., 2017). Inhibition of either CCR5 or CXCR4 leads HIV to shift to a more virulent dual-tropic strain. Therefore dual inhibition of both co-receptors is of paramount importance to improve the therapeutic strategies against HIV infection (Horuk, 2009, Princen et al., 2004). Although numerous selective CCR5 and CXCR4 antagonists have been reported (Grande et al., 2008, Singh and Chauthe, 2011, Chen et al., 2012, Tahirovic et al., 2020), only a few CCR5/CXCR4 dual antagonists have been identified so far (Grande et al., 2019). CCR5 and CXCR4 share an overall similar architecture, and the overlapping regions of the binding pockets pave the way for the identification of dual co-receptor antagonists (Oppermann, 2004).

Maraviroc received marketing approval by the Food and Drug Administration (FDA) as a very potent and selective CCR5 antagonist with a favourable HIV resistance profile. It inhibits RANTES binding to a recombinant CCR5 expressed in the human embryonic kidney (HEK-293) cell line with an IC_{50} value of 5.2 nM (Dorr et al., 2005). Plerixafor (or AMD3100) is a selective CXCR4 antagonist that specifically inhibits SDF-1α binding to CXCR4 (IC_{50} = 12.5 nM) (De Clercq, 2009) Its close analogue AMD3451 (a tetraazamacrocycle) was first reported as a dual CXCR4/CCR5 antagonist (Princen et al., 2004). Alongside, tetraazamacrocycle-based transition metal complexes were shown to act as dual CXCR4/CCR5 antagonist and were endowed with excellent *in vitro* activity against HIV (Hubin et al., 2013). Other dual CXCR4/CCR5 antagonists include, peptide-based triazoles analogues (Tuzer et al., 2013), diterpene derivatives (EC_{50} 0.02 and 0.09 μM against R5 and X4 HIV strains, respectively (Abreu et al., 2014)), and pyrazole derivatives (IC_{50} 3.8 and 0.8 μM against CCR5- and CXCR4-utilizing HIV-1 strains) (Cox et al., 2015). An analogue of the antiparasitic drug suramin NF279 (Giroud et al., 2015), the natural penicillixanthone A (Tan et al., 2019) and a coumarin-based analogue GUT-70 (Kudo et al., 2013) are also known as dual CCR5/CXCR4 antagonists (Fig. 1).

Modern structure-based virtual screening approaches are indispensable in the discovery of novel hits targeting specific proteins and is nowadays a crucial part in the hit-to-lead-optimization phase of drug discovery (Batool et al., 2019, Slater and Kontoyianni, 2019, Mirza et al., 2019). This approach resulted in the discovery of various potent antiviral compounds against viruses such as Ebola (Shaikh et al., 2019), dengue (Zhou et al., 2008), zika (Santos et al., 2019, Yuan et al., 2017), SARS-coronavirus (Nguyen et al., 2011, Mirza and Froeyen, 2020) and influenza (Cheng et al., 2008). The aim of this study was to discover selective CCR5, CXCR4 and dual CCR5/CXCR4 antagonists based on both receptor- and ligand-based virtual screening methods together with molecular dynamics (MD) simulations and binding free energy calculations. The most promising hits were evaluated for CXCR4 and CCR5 antagonism via a Ca^{2+} mobilization assay using U87.CD4.CXCR4 and U87.CD4.CCR5-transfected cell lines. In addition, their anti-HIV-1 activity was evaluated in TZM-bl cells, using NL4.3 (CXCR4 tropic) and BaL (CCR5 tropic) HIV-1 strains.

2. Methods

2.1. Preparation of ligands

Databases of commercially available compounds (MolPort and Interbioscreen databases, ~1.2 million compounds) were used for the virtual screening (VS) and prepared using the LigPrep module of Maestro v.11 (Schrödinger, LLC, New York) software. Possible protonation states were generated using the OPLS3 force field (Roos et al., 2019) at pH 7 ± 2. At most, one stereoisomer was generated per ligand such that the specified chiralities were retained. For the pharmacophore-based screening, the database was converted to the Phase database format with the Generate Phase Database module of Maestro (Dixon et al., 2006, Dixon et al., 2006).

2.2. Preparation of CXCR4 and CCR5 receptors

The VS was specifically performed on CCR5, based on the X-ray crystal structure of CCR5 complexed with maraviroc (PDB ID: 4MBS; A chain) (Tan et al., 2013) was retrieved from the Protein Data Bank (PDB; www.rcsb.org). The co-crystallized ligands, ions and water molecules were removed from the receptor and all hydrogen atoms, missing loops and side chains were added, and bond orders assigned using the Protein Preparation Wizard of Maestro (Sastry et al., 2013). The protonation states of histidine residues were inspected interactively; His88 and His231 were changed to HIE (protonated at Nε atom) and HIP (double protonated), respectively, to optimize the H-bonding network. Restrained minimization using the OPLS3 force field was first applied for hydrogen atoms only and then for heavy atoms

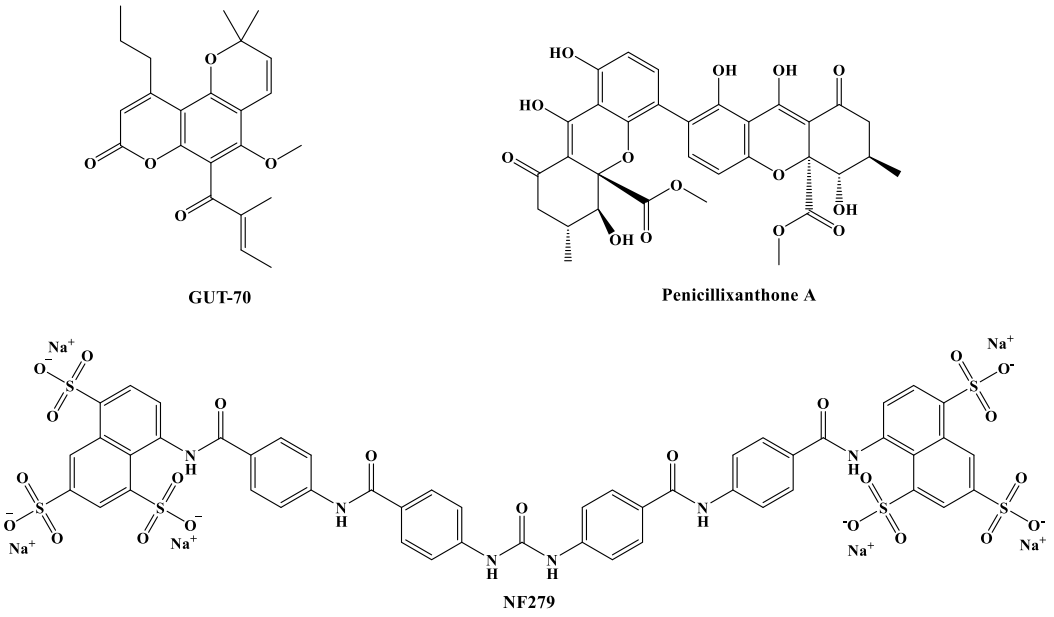

Fig. 1. Structures of dual CCR5/CXCR4 antagonists GUT-70, Penicillixanthone A and NF279.

until non-hydrogen atoms attained an average root-mean-square deviation (RMSD) of 0.3 Å. The top hits from this virtual screening campaign against CCR5 were comparatively docked with CXCR4 in order to discover dual acting CCR5/CXCR4 antagonists. Therefore, the X-ray crystal structure of CXCR4 complexed with an isothiourea derivative (IT1t) (PDB ID: 3ODU) (Wu et al., 2010) was prepared for docking, similarly as described above. In CXCR4, the protonation state of His113 and His281 were changed to HIE and HIP, respectively.

2.3. Receptor-based virtual screening and Prime/MM-GBSA binding free energy

VS by molecular docking was conducted with the Glide module of Maestro (Halgren et al., 2004). The docking site was defined with the Receptor Grid Generation tool of Maestro. The enclosing cubic grid was centered at coordinates (150.03, 108.25, 22.41) and ligand diameter midpoint box was set to 10 Å × 10 Å × 10 Å. The limitation length for ligands to be docked was set to 12 Å. A maximum of five poses per ligand were considered. The Glide high-throughput virtual screening (HTVS) mode was used for the initial docking of the large database after which the top 10% of the hits based on the docking score were chosen and then re-docked using the standard precision (SP) algorithm. Subsequently, 10% of the highest-ranked compounds from this step were redocked using the extra-precision (XP) mode and finally, the top 10% of the Glide XP score-ranked ligands were selected for the binding free energy calculations with the Prime/MM-GBSA module of Maestro (Jacobson et al., 2004). The approximate energies were calculated using the VSGB 2.0 solvation model (Li et al., 2011) and OPLS3 force field, first keeping all binding site residues fixed and then allowing the residues within 5 Å from the ligand to move. Flexible sampling was done by minimization of the complex.

For the best-ranked compounds, molecular property prediction was carried out with Maestro's QikProp module. Besides the Lipinski's rule of five (≤ 2 violations), favorable cell permeability (QPPCaco > 500 nm s^{-1}; QPPMDCK > 500 nm s^{-1}) and acceptable aqueous solubility (-6.5 < QPlogS < 0.5), a series of PAINS filters were applied to eliminate compounds with potential toxicophores.

2.4. Modeling and pharmacophore-based screening

As a second screening approach, pharmacophore modeling was carried out with the Phase module of Maestro (Dixon et al., 2006, Dixon et al., 2006) against CCR5. After preparing the maraviroc-CCR5 crystal complex (PDB ID: 4MBS) with the Protein Preparation Wizard of Maestro, this structure was used for generating the pharmacophore hypothesis. The Nε nitrogen atom of the triazole ring and the amide NH of maraviroc form H-bonds with the hydroxyl groups of Tyr37 and Tyr251, respectively (Fig. 2). In addition, the positively charged nitrogen in the bicyclic ring engages in an ionic interaction with Glu283. Therefore, a H-bond acceptor (A), a H-bond donor (D) and a positive ionic (P) feature were selected as the pharmacophoric features for the hypothesis (Fig. 2). This pharmacophore model was then used to screen through the commercial ligand database in search of matching ligands. The ligands were scored and ranked by the Phase Screen Score according to how well they superimpose on the features associated with the hypothesis. The previously calculated QikProp properties were then used to filter the best-ranked 3000 hit compounds as described above. The 500 ligands that passed the filter were then docked into the maraviroc binding site with Glide using the XP mode and the subsequent Prime/MM-GBSA binding free energy calculation according to the above-described protocol.

2.5. Molecular dynamics simulation and total binding free energy

After a careful analysis of the best-ranked virtual hits, the receptor-bound docked poses of the most promising compounds were subjected to MD simulation to estimate the stability of the binding complexes. All simulations were performed with the AMBER 18 simulation package (Case et al., 2018) using the same MD simulation protocol as described previously (Ikram et al., 2019, Mirza et al., 2019). Each solvated system was minimized stepwise, followed by the heating and equilibration stages. Finally, a production run of 20 ns was performed at 300 K and 1 bar pressure. The time step was set to 2 fs and the trajectory snapshots were saved every 2 ps and analysed using the CPPTRAJ program (Roe and Cheatham Iii, 2013) of AMBER. Moreover, H-bond occupancy was also examined for best compounds over simulation period. The binding free energies (ΔG_{total}) of the most promising hit compounds were calculated using the MM-GBSA (molecular mechanics-generalized Born surface area) method, implemented in AMBER 18. The AMBER ff99SB molecular mechanics (MM) force field (Maier et al., 2015) was used to estimate energy contributions from the atomic coordinates of the ligand, receptor and the complex in a gaseous phase. The total binding free energy is calculated as a sum of the molecular mechanics binding energy (ΔE_{MM}) and solvation free energy (ΔG_{sol}) as given below:

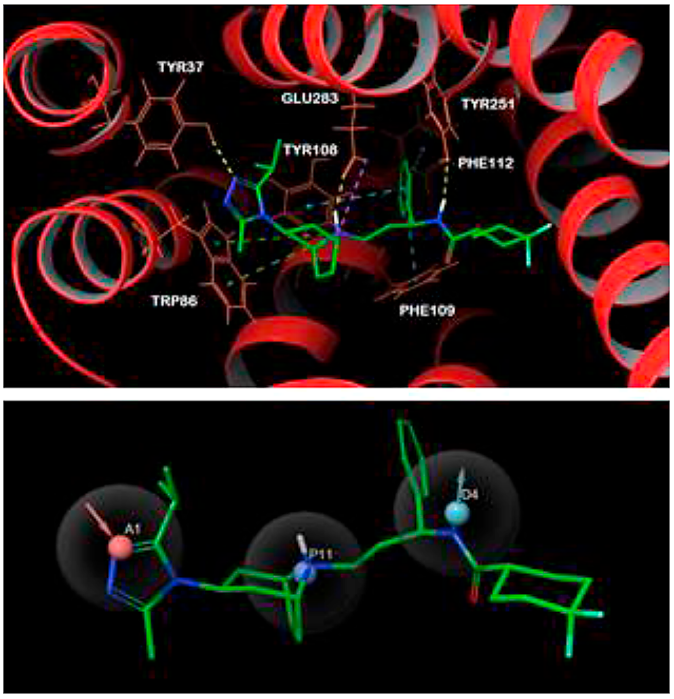

Fig. 2. ***Top:*** Binding mode of maraviroc (green sticks) in the binding pocket of CCR5 (red cartoon): Interaction color code (dashed lines): H-bond – yellow; salt bridge - magenta; π-π – light blue; π-cation - green. Key interacting residues are shown in orange sticks and labelled. ***Bottom:*** Phase generated pharmacophore model. Pharmacophoric features: red sphere for hydrogen-bond acceptor (A); light blue sphere for hydrogen-bond donor (D); blue sphere for the positive ionic (P) feature. The arrows are pointing in the direction of the lone pair. Ligand atom color code: carbon – green; nitrogen – blue; oxygen – red; fluorine – light green. All hydrogen atoms except for maraviroc's polar hydrogens have been omitted for clarity. (For interpretation of the references to color in this figure legend, the reader is referred to the web version of this article.)

$$\Delta E_{MM} = \Delta E_{int} + \Delta E_{ele} + \Delta E_{vdw}$$

$$\Delta G_{sol} = \Delta G_{p} + \Delta G_{np}$$

$$\Delta G_{total} = \Delta E_{MM} + \Delta G_{sol}$$

$$\Delta G_{bind} = \Delta E_{MM} + \Delta G_{sol} - T\Delta S$$

Where, ΔE_{MM} is further divided into internal energy (ΔE_{int}), electrostatic energy (ΔE_{ele}), and van der Waals energy (ΔE_{vdw}), and the total solvation free energy (ΔG_{sol}) is contributed by the sum of polar (ΔG_{p})

and non-polar (ΔG_{np}) components. ΔG_{bind} is the free energy of binding of the ligand evaluated after entropic calculations, which is (TΔS). The MM-GBSA approach has been successfully used in binding free energy calculations (Hou et al., 2011) of antiviral inhibitors (Srivastava and Sastry, 2012, Tan et al., 2006).

2.6. Biological assays

The selected compounds were purchased from MolPort (Riga LV1011, Latvia) in 2 to 5 mg masses. The purity the compounds was greater than 95%.

2.6.1. Anti-HIV replication assay

The most promising compounds resulting from VS were evaluated for antiviral activity by a luciferase assay in TZM-bl cells infected with wild type HIV-1 strains NL4.3 (CXCR4-tropic strain, X4) and BaL (CCR5-tropic strain, R5). AMD3100 (specific CXCR4 antagonist) and maraviroc (specific CCR5 antagonist) were included as best-in-class positive controls. The cellular toxicity of the compounds was also evaluated in TZM-bl cells. The anti-HIV replication assays in TZM-bl cells have been described previously (Luo et al., 2017).

2.6.2. Calcium (Ca^{2+}) mobilization assay

The ability of the compounds to inhibit the Ca^{2+} flux induced by CXCL12 in U87.CD4.CXCR4 cells and by RANTES/CCL5 in U87.CD4.CCR5 cells was investigated via calcium mobilization assays. Intracellular calcium fluxes were measured with the FLIPR Tetra system as described previously (Van Hout et al., 2017). The IC_{50} (i.e., the compound concentration that inhibits the CXCL12-induced CXCR4 signaling or CCL5-induced CCR5 signaling by 50%) was calculated for each compound. The well-known antagonists, AMD3100 (CXCR4) and Maraviroc (CCR5) were used as a positive control.

3. Results

3.1. Virtual screening for the discovery of novel CCR5 and CXCR4 antagonists

To identify novel CCR5 antagonists, two parallel virtual screening campaigns were carried out using both receptor- and a ligand-based (pharmacophore) approaches. A total of ~1.2 million compounds were pre-filtered using a set of selected criteria: the Lipinski Rule of Five ($\leq$ 2 violations), predicted permeability in Caco-2 and MDCK cells ($>$ 500 nm/s) (Bennion et al., 2017), and the predicted IC_{50} value for the blockage of human ether-a-go-go related gene potassium ion (HERG K^+) channel (QPlogHERG value set to -5). HERG K^+ inhibition is a well-known safety issue encountered in the medicinal chemistry optimization of various chemokine receptor antagonists, including maraviroc (Price et al., 2006). As a result, the database was reduced to ~30%, which then underwent the subsequent Glide docking protocol and the compounds were ranked based on XP docking and Prime/MM-GBSA scores. In the pharmacophore-based screening, the top compounds were selected from the pool of the best-ranked 3000 compounds predefined by the pharmacophore hypothesis (as explained in methods). Collectively, 137 compounds were selected and interactively visualized for molecular interactions. Receptor-based virtual hits included the compounds with the lowest (best) binding affinity values and a good interaction profile with the binding site residues of CCR5. Whereas, the main criteria in the pharmacophore-based screening included the potential to establish strong H-bond interaction (salt bridge) with Glu283, π-π stacking interaction with Trp86, and hydrophobic interactions with Tyr108, Ile198, and Tyr198. Furthermore, the visual inspection process contributed to the identification of compounds that revealed significant molecular interactions with the critical binding pocket residues of CCR5 and helped to exclude compounds that showed unrealistic docking conformations.

Among the top hits, 77 were found to follow the set selection criteria and showed strong interactions throughout the 20-ns MD simulations with favourable binding free energies. Although some of these compounds exhibited significantly different binding conformations, all top hits established an extensive interaction network with CCR5. These compounds were further investigated by MM-GBSA calculations and H-bond analysis. After a careful post-MD inspection, 43 compounds were selected based on the following criteria; (1) overall backbone stability of the protein/ligand complex, (2) electrostatic (ΔE_{ele}) and van der Waals (ΔE_{vdw}) interaction energy, (3) H-bonds occupancy, and (4) binding pocket residual contribution towards ligands. All these 43 hits were comparatively docked at CXCR4 receptor to investigate their potential for dual CCR5/CXCR4 antagonists (Grande et al., 2019). As described earlier, both CCR5 and CXCR4 share marked similarities in their overall structures and in their active site geometry. These similarities include the presence of seven transmembrane domains with a high number of proline residues, a C-terminal threonine and serine-rich cytoplasmic region, four extracellular loops with a high number of cysteine residues and an N-terminal extracellular domain. The regions of the binding pockets contain critically important conserved residues which might allow CCR5 and CXCR4 to host the same ligand. Based on these evidences, we specifically sorted out potential hits and 27 structurally diverse compounds were purchased and tested for their anti-HIV activity (Fig. S1)

3.2. Calcium (Ca^{2+}) mobilization studies

The Ca^{2+} mobilization assay allowed to evaluate the antagonistic activity (i.e., the potency to inhibit the RANTES/CCL5 and SDF-1/CXCL12-induced calcium mobilization) of the selected compounds. Both RANTES (natural CCR5 ligand) and CXCL12 (natural CXCR4 ligand) produced a robust transient increase of cytosolic Ca^{2+} flux in U87.CD4.CCR5 and U87.CD4.CXCR4 cells, respectively. Among the tested compounds, compounds **3, 6,** and **27** showed antagonistic activity and dose-dependently inhibited the intracellular-induced Ca^{2+} flux (Table 1). The structures of these compounds are shown in Fig. 3. Compound **3** at 100 μM completely blocked the CXCL12 induced Ca^{2+} signaling in U87.CD4.CXCR4 (IC_{50} = 38.34 μM) and CCL5 induced Ca^{2+} signaling in U87.CD4.CCR5 (IC_{50} = 64.56 μM) cells. At 20, 4, and 0.8 μM, compound **3** inhibited the CXCL12-induced Ca^{2+} flux (CXCR4 mediated) by 15, 11 and 9%, respectively. On the other hand, it inhibited the CCL5-induced Ca^{2+} flux (CCR5 mediated) to a lesser extent (60% inhibition at 100 μM) in respective cells. Thus, compound **3** clearly exhibited dual CCR5/CXCR4 antagonism.

Compound **6** inhibited the CXCL12-induced Ca^{2+} flux with an IC_{50} value of 61.51 μM. At a concentration of 100 μM compound **6** did not affect the Ca^{2+} flux evoked by RANTES, indicating that compound **6** was devoid of CCR5 antagonistic activity. Compound **27** displayed promising selective CCR5 antagonistic activity as it dose-dependently inhibited the CCL5-induced intracellular Ca^{2+} flux by 96, 76 and 52% at concentrations of 100, 20, and 0.8 μM, respectively. No inhibition of the Ca^{2+} response elicited by the action of CXCL12 on the CXCR4 receptor was observed up to 100 μM.

3.3. Anti-HIV activity

The ability of the compounds to inhibit the cytopathogenic effect induced by NL4.3 (CXCR4-tropic strain, X4) and BaL (CCR5-tropic strain, R5) HIV-1 strains was further evaluated in TZM-bl cells (Table 1). AMD3100 and maraviroc were used as positive controls for HIV-1 NL4.3 and HIV-1 BaL, respectively. Both drug controls were very efficient in inhibiting NL4.3, and BaL strains in TZM-bl cells with EC_{50} values of 0.93 and 3.99 nM, respectively. Some of the selected compounds showed anti-HIV activity against both HIV-1 strains with EC_{50} values in micromolar range, while a few compounds were found significantly toxic (CC_{50}). Compounds **3, 24** and **25** displayed promising

Table 1
Anti-HIV-1 activity, Ca^{2+} chemokine signaling inhibition, MM-GBSA and Glide XP score of the selected compounds.

Compound	TZM-bl Toxicity CC_{50}	NL4.3 CXCR4 EC_{50}	U87.CD4 CXCR4 IC_{50}	BaL CCR5 EC_{50}	U87.CD4 CCR5 IC_{50}	MM-GBSA CCR5 kcal/mol	XP CCR5 kcal/mol
1	6.33	>6.33	>100	>6.33	>100	-65.14	-9.27
2	1.25	0.14	61.9	0.29	>100	-60.15	-8.54
3	37.24	20	39.1175	23.44	64.562	-65.68	-8.91
4	>100	>100	>100	>100	>100	-34.25	-8.41
5	87.19	51.71	>100	47.56	>100	-52.7	-9.1
6	68.40	61.62	61.51	46.57	>100	-56.48	-8.57
7	>100	>100	>100	>100	>100	-62.11	-9.1
8	>100	>100	>100	>100	>100	-41.28	-8.07
9	>100	53.78	>100	64.28	>100	-34.88	-9.57
10	>100	>100	>100	>100	>100	-36.59	-8.77
11	>100	>100	>100	>100	>100	-33.03	-9.12
12	>100	>100	>100	>100	>100	-44.6	-8.62
13	8.43	7.55	>100	>8.43	>100	-56.59	-8.81
14	73.91	>73.91	>100	>73.91	>100	-57.95	-8.09
15	> 100	41.13	>100	>100	>100	-48.56	-9.04
16	18.14	14.22	>100	10.62	>100	-33.84	-9.01
17	100	>100	>100	>100	>100	-40.19	-8.39
18	>100	>100	>100	>100	>100	-44.92	-9.53
19	54.88	>54.88	>100	35.63	>100	-43.87	-8.8
20	8.46	>8.46	>100	>8.46	>100	-45.46	-7.51
21	>100	64.33	>100	>100	>100	-51.85	-8.57
22	>100	>100	>100	>100	>100	-42.26	-9.1
23	71.82	42.11	>100	50.80	>100	-49.57	-8.67
24	33.01	27.89	>100	24.25	>100	-49.38	-10.2
25	25.16	18.26	>100	16.29	>100	-43.04	-10.91
26	>100	41.48	>100	57.80	>100	-38.17	-8.15
27	>100	>100	>100	>100	10.642	-65.29	-9.12
AMD3100 (nM)	>1000	0.93	85	-	-	-	-
Maraviroc (nM)	>1000	-	-	3.99	1.6	-	-

The values of CC_{50}, EC_{50} and IC_{50} are in micromolar if not otherwise stated. The results represent the mean of four readings.

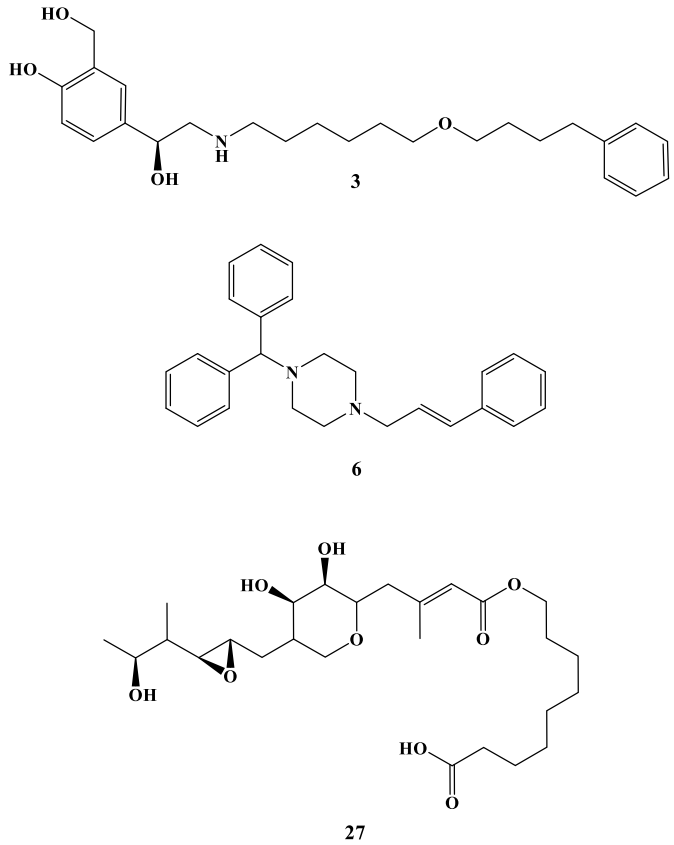

Fig. 3. Structures of identified dual CXCR4/CCR5 antagonist **3**, CXCR4-specific antagonist **6**, and CCR5-specific antagonist **27**.

anti-HIV-1 activity by inhibiting CCR5-tropic (R5) HIV-1 infection with EC_{50}*'s* of 23.44, 24.25, and 16.29 μM, and CXCR4-tropic infection with EC_{50} of 20, 27.89 and 18.26 μM, respectively. These compounds showed low to moderate cytotoxicity (CC_{50} > 25 μM). Compounds **2, 13**, and **16** showed promising anti-HIV activity with EC_{50} of 0.29, 8.43, and 10.62 μM against BaL, and EC_{50} of 0.14, 7.55, and 14.22 μM against NL4.3, but were found to be toxic in TZM-bl cells (CC_{50} 1.25 to 18.43 μM). Among the other compounds, **5, 6, 9, 14, 19, 23**, and **26** showed weak anti-HIV activity against BaL (EC_{50} ranging from 35.63 to 64.28 μM), and NL4.3WT (EC_{50} values between 41.48 and 64.33 μM), with no significant toxicity (CC_{50} >54.88 μM). Two compounds, **15** and **21** were only active against HIV-1 NL3.4 strain and displayed weak anti-HIV activity (EC_{50} 41.13 and 64.33 μM; CC_{50} >100 μM), while no activity was observed against the BaL strain at 100 μM, suggesting that these two compounds could be selective inhibitors against the NL4.3 HIV-1 strain in TZM-bl cells.

3.4. Binding mode analyses

The calcium mobilization clearly indicated that compounds **3, 6**, and **27** bind to the host co-receptors. Although compound **27** showed an IC_{50} value in the low micromolar range as CCR5 antagonist, no antiviral activity was observed even at the highest tested concentration of 100 μM. The predicted binding modes of compounds **3** (CCR5/CXCR4 antagonist), **6** (CXCR4), and **27** (CCR5) were investigated to obtain an atomic understanding inside the binding pocket. For all three compounds, the MD simulation time was further extended from 20 to 50 ns to enhance the investigations on the stability of the complexes and the compounds' binding energy contributions.

3.4.1. Experimental correlation

The statistical correlation was also evaluated between the average Amber/MM-GBSA total binding free energy (ΔG_{total}) at the co-receptors

Table 2
The effect of the inclusion of entropy on the free energy of binding for CCR5 and CXCR4 complexes with compound 3. The normal-mode analysis was performed to evaluate the conformational entropy change (−TΔS) upon ligand binding.

Complex	Exp. IC_{50}	ΔG_{exp} [1] (kcal/mol)	Average MM-GBSA ΔG_{total} (kcal/mol)	Standard error (kcal/mol)	Conformational entropy change (-TΔS) (kcal/mol)	Absolute binding energy ΔG_{bind} [2] (kcal/mol)
CXCR4/3	38.34	-6.3	-48.11	0.24	-29.4	-18.71
CCR5/3	64.56	-5.9	-68.83	0.19	-41.7	-27.13
CXCR4/6	61.51	-5.9	-54.31	0.12	-35.02	-19.29
CCR5/27	10.64	-7	-65.29	0.2	-48.32	-16.97

[1] $\Delta G_{bind} = \Delta G_{total} - T\Delta S$
[2] $\Delta G_{exp} = -RT \ln IC50$

and the experimental IC_{50} values from Ca^{2+} mobilization assay (Table 2). The estimated ΔG_{total} extracted from the last 20 ns simulation of the dual CXCR4/CCR5 antagonist **3** (-48.11/-68.83 kcal/mol) correlated with the experimentally determined IC_{50} values of CXCR4 (IC_{50} = 38.34 μM) and CCR5 (IC_{50} = 64.56 μM). The relative non-entropic ΔG_{total} values were used for comparison between similar co-receptors.

Similarly, compound **6** showed ΔG_{total} of -54.31 kcal/mol statistically correlated to its experimental IC_{50} value (61.51 μM). On the other hand, compound **27** showed weak correlation (-65.29 kcal/mol) with the experimentally determined IC_{50} value (10.64 μM). Inclusion of conformational entropy changes (-TΔS) in the MM-GBSA ΔG_{total} values to get absolute binding free energies (ΔG_{bind}) did not change the order of binding affinities for compound **3** against CXCR4 (ΔG_{bind} = -18.71 kcal/mol) and CCR5 (ΔG_{bind} = -27.13 kcal/mol). Compound **6** showed ΔG_{bind} of -19.29 kcal/mol, whereas, compound **27** showed a better correlation with the inclusion of entropy (ΔG_{bind} = -16.97 kcal/mol). In addition to MM-GBSA calculations, we also determined the per-residue decomposition to analyse the energy contribution of binding pocket residues towards ligand's binding. The predicted experimental binding affinity (ΔG_{exp}) deduced from IC_{50} showed poor correlation with the $\Delta G_{bind,}$ expect compound **27** which fairly correlated with ΔG_{exp} (-7 kcal/mol).

3.4.2. Stability of complexes

The stability analysis of the top-ranked compounds against CCR5 is diagrammatically illustrated in (Fig. 4, S2-S3). Overall, all 27 tested compounds occupied the bottom of the CCR5 binding cavity defined by the residues of the transmembrane (TM) helices (1, 2, 3, 4, 5 and 7), and these binding poses were supported by the co-crystallized conformation of maraviroc (Fig. 4A). Moreover, the protonated nitrogen of the compounds identified through the pharmacophore-based hypothesis was found in the close vicinity of the negatively charged Glu283, and most of these nitrogen atoms engaged in salt bridge interactions. All compounds exhibited excellent binding energies against CCR5 as indicated via the energy plot, where compounds **3, 6,** and **27** ranked among the top, albeit no inhibition of Ca^{2+} flux evoked by RANTES was observed for **6** (Fig. 4B). The stability of these compounds inside the deep binding cavity of the corresponding co-receptors revealed convergence in RMSD values (Figure S2). Compound **27** reached an equilibrium value of ~1.5 Å (relative to the equilibrated position of the ligand) somewhat late than the others, at around 20 ns, due to its flexible fatty acid side-chain (Figure S2). Compound **6** adopted a favourable conformation inside the CXCR4 binding pocket at around 13 ns and the dual antagonist **3** displayed consistently stable binding at both co-receptors already from the early steps of the simulation (~ 2-3 ns) (Figures S2). The stable RMSD value in the last ~ 30 ns was evident from the stable molecular interactions governed by the ligand inside the respective binding site of the co-receptors. Furthermore, the TM helices of CXCR4 and CCR5 also exhibited significant stability as observed from the root-mean-square fluctuations (RMSF < 1 Å), although TM5, which is connected to TM4 by the largest extracellular loop ECL2, showed somewhat larger fluctuations (around 2 Å) (Fig. 4A and S3).

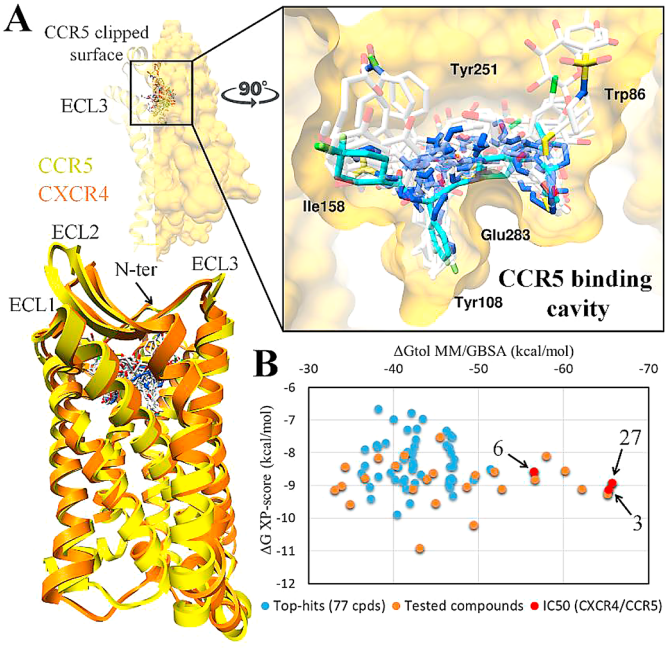

Fig. 4. Molecular modelling analysis of the HIV-1 entry co-receptors. **(A)** Overlay representation of CCR5 (golden ribbon and surface presentation; PDB ID: 4MBS) and CXCR4 (orange ribbon; PDB ID: 3ODU) with all 27 virtual screening hits in the CCR5 binding site. The docked poses of the hits (white carbons, sticks presentation) are zoomed in together with the co-crystalized maraviroc (cyan carbons, sticks presentation) in the CCR5 binding pocket. Atom colour code: red – oxygen; blue – nitrogen. The positions of the most commonly interacting binding pocket residues are labelled. **(B)** Scatter plot of the Glide XP docking score vs Amber/MM-GBSA values of all 77 hits. Tested compounds are coloured orange, while the most significant three compounds, 3, 6 and 27 are coloured red and labelled. (For interpretation of the references to color in this figure legend, the reader is referred to the web version of this article.)

The binding cavity of both co-receptors is mostly hydrophobic due to the presence of a relatively large number of nonpolar amino acids. The analysis of the binding interactions demonstrated that the stability of the compounds inside the binding pocket of CXCR4 and CCR5 is mostly governed by π-stacking and H-bond interactions (Fig. 5A-D). For further in-depth understanding of interactions, H-bond occupancy was also recorded (distance ≤ 3 Å; angle ≥120°) throughout the 50 ns simulations (Fig. 5E). Per-residue decomposition was also performed for the key residues involved binding the ligands.

In **27**/CCR5 complex, the interactions were mainly governed by multiple H-bond interactions with the binding site residues. Compound **27** contains a short flexible fatty acid side-chain (9-hydroxynonanoic acid) linked to monic acid by an ester linkage. As evident from the molecular interactions, compound **27** established a network of H-bonds over a period of 50 ns and adopted a more favourable conformation inside the binding cavity (Fig. 5A). The monic acid moiety reached deep

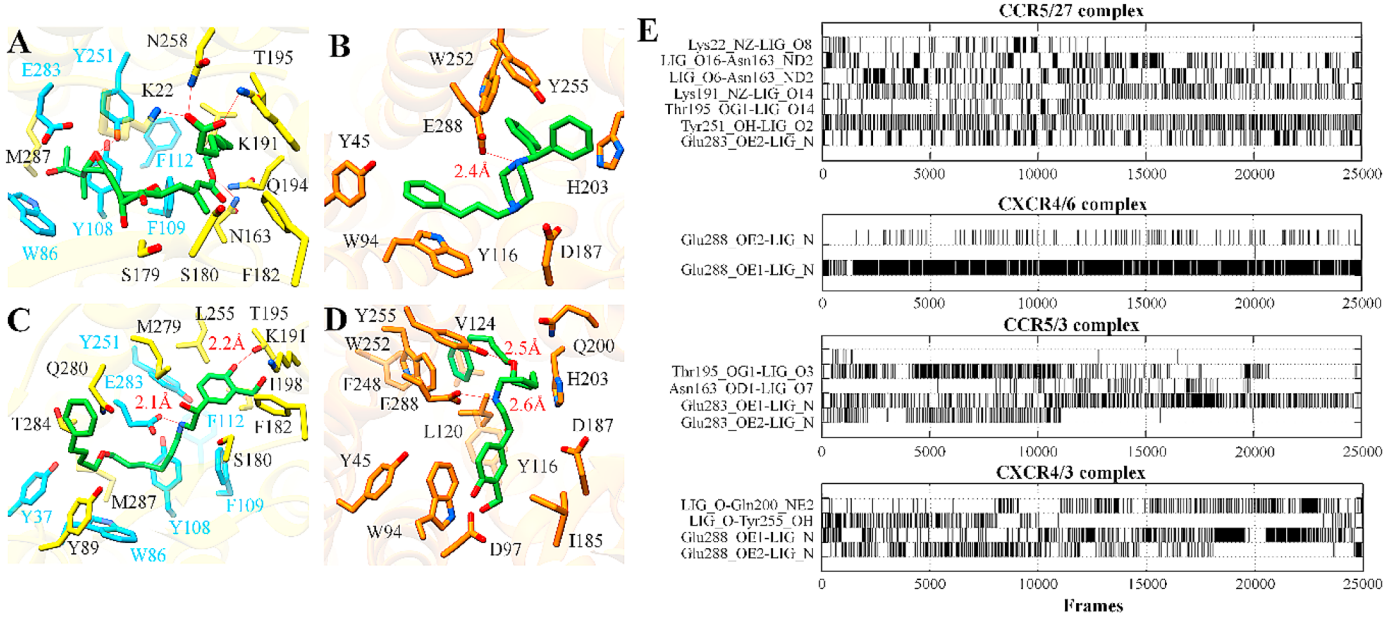

Fig. 5. MD simulated conformation of potential antagonists, **27 (A), 6 (B)** and **3 (C** and **D)**, inside the binding pocket of CCR5 (golden sticks) and CXCR4 (orange sticks). The residues that were considered important interaction partners when selecting the best hits from the pharmacophore-based screening are shown as cyan sticks. All binding site residues are labelled and hydrogen bonds are denoted as red dashed lines. **(E)** Hydrogen bond occupancy of the key hydrogen bonds in each ligand (LIG)-receptor complex extracted from 25000 snapshots (after every 2 ps) along the 50-ns simulation trajectory. (For interpretation of the references to color in this figure legend, the reader is referred to the web version of this article.)

into the pocket and formed hydrophobic interactions with four important aromatic residues, including Trp86, Tyr108, Phe109, and Tyr148. Here, the epoxide linker established a H-bond (33.4%; average distance, 2.61 Å) with the side-chain oxygen atom of Tyr251. The ester linkage established two strong H-bonds with Asn163 (average distance < 2.5 Å) with an occupancy of 20.4% and 22.38%. The monic acid with its ester linkage occupied most of the volume of the binding cavity and bound in an orientation wherein the terminal oxygen atoms of nonanoic acid positioned towards the positive potential created by the side chains of Lys22, Lys191. Herein, a network of four H-bonds was formed, two with the side-chain nitrogen atom of Asn163 (average distance < 2.7 Å; occupancy, 36.2% and 12.3%) and the remaining two H-bonds with Lys191 (41.37%) and Lys22 (11.8%). The stable RMSD value of compound **27** after 20 ns was evident from this network of interactions established by the nonanoic acid's side chain (Fig. 5A). The per-residue decomposition analysis revealed favourable binding free energy contributions (< -1.5 kcal/mol) with Trp86, Tyr108, Phe109, Tyr148, whereas the interaction with Glu283 revealed a positive value due to the desolvation effect.

In the CXCR4/**6** complex, the phenyl rings on either side of the molecule were fluctuating during the simulation, with especially the terminal phenyl moiety connected to the aliphatic carbon side chain, whereas the central piperazine ring remained stable in its position. As shown in Fig. 5B, the terminal side-chain benzene established a strong π-π stacking with Trp94 and revealed the most favourable energy decomposition value of -4.6 kcal/mol as compared to the other π-π stacking interactions (with Tyr108 and Phe109). This π-π stacking interaction was found completely missing with Trp86 in the **6**/CCR5 complex because the molecule was flipped inside the binding cavity of CCR5 (Figure S4), which might explain the lack of activity against CCR5. Moreover, the oxygen atom of the side-chain carboxylic acid of Glu288 formed a strong and well populated (82.7%) salt-bridge (average distance, 2.47 Å) with the protonated nitrogen atom of the piperazine ring of compound **6**, which could stabilize the central piperazine ring. Glu288 also showed a favourable binding free energy contribution of -3.37 kcal/mol.

The dual CCR5/CXCR4 antagonist **3** contains a salicyl alcohol moiety, a chiral β-hydroxyl group, a secondary amine, and an ether-linked aryloxyalkyl sidechain. The nonpolar side chain facilitated binding with the hydrophobic binding cavity of the co-receptors. The protonated nitrogen of secondary amine in **3** retained similar spatial coordinates in both complexes and established well-populated salt-bridge (64.2 and 58.5%; average distance, 2.15 and 2.64 Å) with the glutamate residue of CCR5 (Glu283) and CXCR4 (Glu288) at respective sites (Fig. 5C-E). The salt-bridge with glutamate provided an anchor point for a dual antagonist to extend in both directions. On one side, the aryloxyalkyl tail reached deep into the binding cavity of CCR5, where the terminal phenyl ring formed hydrophobic interactions with Tyr37, Tyr89, Gln280, Thr284 and Met287 (Fig. 5C). Whereas, the phenyl ring formed a π-π interaction with Trp252 and established one H-bond with Tyr255 (46.4%; average distance, 2.55 Å) in CXCR4 (Fig. 5D). On the other side, the two hydroxyl groups of the salicyl alcohol moiety established H-bonds with Thr195 of CCR5 (35.1%; average distance, 2.23 Å), although no stable H-bond was observed by this group in CXCR4, except an additional stacking interaction with Trp94. Among the interacting residues, Tyr108 (CCR5) and Tyr116 (CXCR4) showed favourable interactions, while Glu283 (CCR5) and Glu288 (CXCR4) revealed a slightly negative value.

3.5. Performance of the MM-GBSA approach

The EC_{50} values of the different compounds against CCR5 and CXCR4 were correlated quantitatively with the Amber/MM-GBSA binding energy values derived from the MD simulations in order to assess the performance of the calculations. For each MD simulated co-receptor complex with the bound ligand, a total of 5000 snapshots (every 4 ps) were generated. The ΔG_{total} values were calculated at 10 different time scales (0-2 to 0-20 ns) and compared with the experimental EC_{50} values. Table 3 tabulates average ΔG_{total} values for CCR5 at different time scales (0-2 to 0-20 ns) of MD simulation along with the pEC_{50} (-log of EC_{50}) values. The quantitative correlation between ΔG_{total} and experimental pEC_{50} values at the shortest time scales (0-2 ns and 0-4 ns) was rather poor (R^2 = 0.347 and 0.285), albeit a gradual increase in correlation was observed with larger time scales (> 0-12 ns

Table 3
Comparison of experimental pEC_{50} (-log of EC_{50}) and MM-GBSA binding free energy (ΔG_{total}) values of CCR5 antagonists at various time scales (0-2 to 0-20 ns) of MD Simulation along with Correlation Coefficient (R^2).

Active cpds	pEC50	MMGBSA (Amber)	0-2 ns	0-4 ns	0-6 ns	0-8 ns	0-10 ns	0-12 ns	0-14 ns	0-16 ns	0-18 ns	0-20 ns
cmp3	4.69	-58.51	-68.7	-68.1	-70.56	-69.65	-67.43	-66.71	-65.14	-64.46	-65.1	-65.83
cmp5	4.3	-79.45	-51.41	-53.27	-52.16	-52.69	-53.3	-52.38	-54.21	-52.03	-52.17	-52.7
cmp6	4.33	-97.21	-60.11	-57.92	-55.24	-54.81	-52.7	-50.5	-51.66	-53.17	-55.5	-55.8
cmp9	4.19	-91.24	-61.24	-60.4	-61.01	-59.51	-56.91	-55.06	-54.2	-53.31	-54.31	-56.98
cmp14	4.13	-86.17	-48.75	-49.17	-50.94	-50.14	-51.56	-51.9	-51.74	-52.23	-51.2	-53.25
cmp16	4.9	-55.48	-58.47	-57.12	-58.67	-57.29	-56.23	-55.1	-56.71	-56.25	-58.06	-61.8
cmp19	4.44	-76.15	-55.78	-51.2	-51.2	-53.81	-54.6	-54.27	-53.13	-53.48	-53.15	-52.75
cmp23	4.29	-91.23	-49.7	-49.08	-50.11	-51.57	-52.51	-49.2	-48.21	-49.87	-52.78	-51.41
cmp24	4.6	-86.46	-62.42	-64.43	-62.18	-63.1	-63.03	-62.88	-59.91	-58.71	-57.97	-58.01
cmp25	4.78	-69.04	-60.11	-59.2	-62.61	-59.1	-60.19	-61.2	-59.91	-58.97	-59.84	-61.25
cmp26	4.23	-50.57	-53.22	-54.72	-55.24	-49.21	-50.77	-47.79	-49.25	-50.8	-52.39	-53.09
R		0.51	-0.59	-0.53	-0.61	-0.62	-0.66	-0.68	-0.73	-0.75	-0.79	-0.79
R (squared)		0.26	0.35	0.29	0.37	0.38	0.44	0.46	0.54	0.56	0.62	0.63

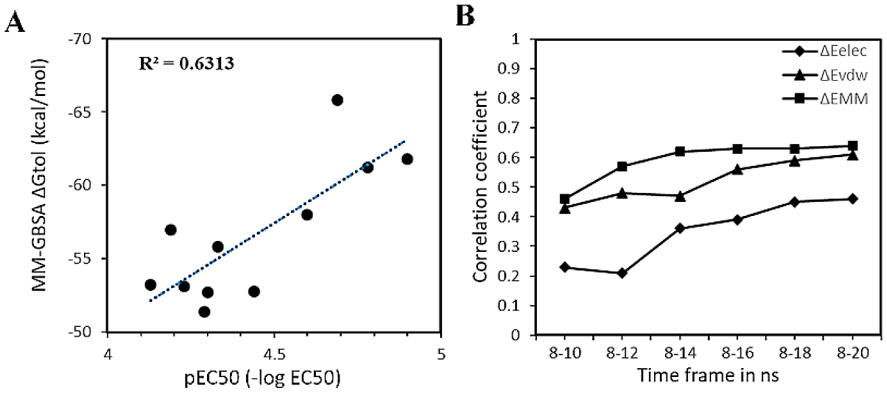

Fig. 6. Performance of the Amber/MM-GBSA approach. (A) Correlation plot between the MM-GBSA binding free energy (ΔG_{total}) against CCR5 and pEC50 (-log of EC_{50}) for compounds in CCR5-tropic strain, R5, that showed low or medium antiviral activity (compounds with no antiviral activity are excluded). (B) Plot of correlation coefficient (R^2) values obtained by correlating ΔE_{MM} and their components (ΔE_{ele} and ΔE_{vdW}) with experimental EC_{50} values at various time scales (8-10 to 8-20 ns) of MD simulations. [ΔE_{ele} is electrostatic energy as calculated by the molecular mechanics (MM) force field and Δ_{vdW} is van der Waals contribution from MM].

and above). The initial poor correlation was due to the event of a single conformation of the protein-ligand complex, which did not incorporate the flexibility in the beginning of the simulation. This underlying phenomenon was also evident from the correlations obtained from the docking scores (Glide XP) alone, which showed poor R^2 value (0.353) (Figure S5). Afterwards, improved correlations were observed with a longer time scales of 0-18 (R^2 = 0.622) and 0-20 ns (R^2 = 0.631) (Table 3, Fig. 6).

The overall trend of ligand RMSD trajectories of most complexes (except for few) showed stability after ~8 ns (8-20 ns), which is rationalized through the electrostatic and vdW interaction energies. Consequently, the plot of ΔE_{MM} components (ΔE_{ele} and ΔE_{vdW}) with respect to MD simulations at various time scales (8-10 to 8-20 ns) were correlated separately with experimental pIC_{50} values, as shown in Fig. 6.

Overall, the components showed a reasonable correlation which improved at higher simulation times, where, ΔE_{vdW} displayed better correlation at 8-18 ns and 8-20 ns timescales (R^2 = 0.59 and 0.61) as compared to ΔE_{ele} (R^2 = 0.451 and 0.463) on the final estimated ΔE_{MM} (R^2 = 0.632 and 0.645). For CXCR4, no satisfactory correlation was found except 0.471 at 0-20 ns time scale (data not shown).

4. Discussion

CCR5 and CXCR4 are both important co-receptors involved in the HIV-1 entry process (Grande et al., 2019, Shepherd et al., 2013, Princen et al., 2004, Zhukovsky et al., 2013). The CCR5 binding cavity is much deeper and open, while the entrance to the active site of CXCR4 is relatively covered having a strong negative charge on the surface as compared to CCR5 (Tan et al., 2013). A highly negative surface charge density across the binding site makes CXCR4 atypical among the chemokine receptors and this difference is evident form the structural attributes of the CXCR4-specific inhibitors. Despite the substantial difference in the surface electrostatic potential, many compounds have been reported against both co-receptors (Princen et al., 2004, Hubin et al., 2013, Cox et al., 2015, Seibert and Sakmar, 2004, Taylor et al., 2017).

Comprehensive virtual screening experiments were carried out to investigate the multiple topographies of the CCR5 binding pocket using both receptor- and ligand-based approaches. The top hits from the CCR5 virtual screening campaign were afterwards docked in the binding cavity of CXCR4 to investigate the dual antagonism of these compounds. 27 Compounds were selected for biological evaluation, from which three displayed promising activity. Compound **3** is salmeterol, a β_2-adrenergic receptor agonist acting as a dual CXCR4/CCR5 antagonists. Compound **6** is the antihistamine drug cinnarizine with CXCR4 antagonistic potency and compound **27** is the antibiotic mupirocin displaying potent CCR5 antagonism. To date, no antiviral activity of these compounds has been reported, except for moderate activity of salmeterol against the dengue virus (Medigeshi et al., 2016). Although, the pharmacological properties of these compounds have already been explained in the previous studies, very briefly, salmeterol is indicated to improve airflow in chronic obstructive pulmonary disease, and asthma. It falls under the category of long acting β-2 adrenergic receptor inhibitors with an elimination half-life of 5.5 hr when administered via pulmonary route. This long-acting feature of salmeterol is considered associated with its ability to bind with both active and exo-sites of the receptor. A blood maximum concentration of salmeterol is achieved within 15 min of pulmonary administration (Cazzola et al., 2002). CYP3A4 is considered predominantly involved in the metabolism of salmeterol through α-hydroxylation. Some frequently known adverse effects of salmeterol may include hyperlactatemia, metabolic acidosis, depression, anxiety, hypophosphatemia, and hypokalemia (Manara et al., 2012). Although, a 6-month long clinical

trial of salmeterol have proved satisfactory in context of safety profile (Rosenthal et al., 1999). In context of these findings and keeping in view the serious side-effects of antiretroviral therapy, it could be most likely stated that further development and repurposing salmeterol for HIV treatment could serve a promising approach.

Cinnarizine is an antihistaminic compound used for motion sickness and vestibular disorders and is also considered as a nootropic agent (Wilder-Smith et al., 1991, Nicholson et al., 2002). It is a long-known calcium channel blocker with slight potency towards certain dopamine receptors (Brücke et al., 1995). After oral administration, a maximum plasma concentration approaches in nearly 3 h with elimination half-life of 3 to 4 h (Castaneda-Hernandez et al., 1993). Its six metabolites are known, which are produces via different of CYPs (Allewijn, 1968). Although, cinnarizine has long been used in clinical practice with considerable tolerance but concerns has been raised for its association with drug-induced acute and chronic parkinsonism, linked to its ability to interact with dopamine receptors (Teive et al., 2004). On the other hand, long-term clinical trials up to 4-month have demonstrated reasonable safety (Barber et al., 1980) suggesting its beneficial application for further development as an anti-HIV agent.

Mupirocin, also known as pseudomonic acid A, is a natural produced by *Pseudomonas fluorescens* that can inhibit bacterial isoleucyl-tRNA synthetase (Parenti et al., 1987). It is found effective against many gram-positive bacteria and some gram-negative bacteria. The presence of epoxide residue in mupirocin makes it prone to extensive metabolism quickly converting it into inactive monic acid, which makes its applications limited to topical antibacterial ointment (Parenti et al., 1987). Its elimination half-life ranges between 20 and 40 min after an intravenous administration (Pappa, 1990). Due to this short half-life and lack of detailed pharmacological data from parenteral or oral administration requires extensive further experimentation for the use of mupirocin against HIV.

Compounds **3, 6** and **27** showed highly significant Amber/MM-GBSA (calculated) binding energy values during screening. Through molecular modelling studies, the compounds were found well-fitted inside the binding site of both co-receptors and remained stable throughout the MD simulation period. During MD simulations, the compounds remained in a close proximity to a negatively charged glutamate residue in the respective co-receptors. Molecular interactions of compounds **3** and **6** were in line with the pharmacophore hypothesis and the co-crystalized complexes of CCR5/maraviroc (Tan et al., 2013) and CXCR4/IT1t (Wu et al., 2010), respectively. The protonated nitrogen atoms of the tropane group of maraviroc engaged in a salt-bridge interaction (2.78 Å) with Glu283 of CCR5, while the protonated nitrogen of the imidazo-thiazole moiety (N1) of IT1t shows a salt-bridge interaction (2.8 Å) with Glu288 of CXCR4. Likewise, the piperazine nitrogen of compound **6** and the secondary amine of compound **3** established a consistent salt-bridge interaction over a period of 50 ns with the respective glutamates. The importance of the glutamate residue deep inside the active site in the stabilization of the complexes has been reported previously (Castonguay et al., 2003, Dragic et al., 2000, Govaerts et al., 2003, Nishikawa et al., 2005, Tsamis et al., 2003, Heredia et al., 2018, Neves et al., 2010) and, therefore, Glu288 of CXCR4 and Glu283 of CCR5 are important residues for structure-based drug discovery of CXCR4 and CCR5 antagonists. In addition, both compounds engaged in significant non-polar interactions with the corresponding hydrophobic residues of the respective co-receptors, and these interactions are supported with previous mutagenesis and modelling studies (Tan et al., 2013, Wu et al., 2010, Garcia-Perez et al., 2011, Scholten et al., 2012). Compound **27**, the most promising compound after receptor-based screening (IC_{50} = 10.64 μM), showed a significant H-bond interaction profile with the residues lining the binding pocket of CCR5, as reported also for maraviroc (Tan et al., 2013, Garcia-Perez et al., 2011).

Compound **6** did not inhibit the calcium flux induced by RANTES in U87.CD4.CCR5 cells, despite the significant MM-GBSA binding energy with CCR5 (ΔG_{total} = -56.48 kcal/mol). The difference in electrostatic potential of the entrance of the binding site may provide the reason to this discrepancy, which has long been recognized between R5 and X4 strains (Fouchier et al., 1992), and is supported by numerous mutational studies (De Jong et al., 1992, Cardozo et al., 2007, Shimizu et al., 1999, Hatse et al., 2001). CCR5 bears a neutral to positive electrostatic surface at the binding site entrance, with a deep negatively charged binding pocket, which might hinder the cationic piperazine moiety of compound **6** (Dragic et al., 2000). CXCR4 has a strongly negative surface charge due to a highly negative N-terminus that can favourably accommodate compound **6** (Loetscher et al., 1994). Likewise, compounds **15** and **21**, having relatively similar electronegative cyclic nitrogen atoms, showed selective anti-HIV activity against X4 HIV-1 strain (IC_{50} of 41.13 and 64.33 μM, respectively). Furthermore, the binding pocket of the H_2-histamine receptor (PDB ID: 6BQG), the primary target of cinnarizine (Peng et al., 2018), has a similar, negatively charged surface (Figure S6), which is in agreement with the selective binding of compound **6** with CXCR4. In contrast, compound **27** possesses an overall negative charge (Hill, 2002) and is a potent CCR5 antagonist, lacking activity against CXCR4.

Per-residue decomposition analysis revealed binding free energy contributions by important binding site residues involved in electrostatic and vdW interactions. Among the residues that were found to stabilize the complex formation, glutamate residues produced positive decomposition values for compounds **3** and **27**. This was due to the contribution of unfavourable solvation energy by blocking out a sufficient amount of solvent that might stabilize these negatively charged glutamates. However, due to the presence of long carbon chains in **3** and **27** reduced the solvent exposure of glutamate residues inside the binding cavity resulting in a more favourable value. Compound **6** showed a fairly negative energy value for glutamate interaction due to the presence of two protonated nitrogen atoms of the piperazine ring, which counteracted the desolvation effect. This more negative per-residue decomposition value of Glu288 in CXCR4 is supported by the evidence from Taylor et al. (2017). They changed the protonated piperidine ring (Cox et al., 2015) to a doubly protonated piperazine ring aiming at increasing the electrostatic interactions, hence counteracting the desolvation effect.

Although the identified compounds were less active against CCR5 and CXCR4 as compared to the positive controls maraviroc and AMD300, it should be underlined that these compounds are directly derived from virtual screening approaches without any further optimization. According to the literature, this is the first account of the activities of these compounds against CCR5 and CXCR4. Moreover, the structural pharmacophores that are present in compounds **2, 3, 6,** and **27** were not observed in the previously reported CCR5 and CXCR4 antagonists. Pyrimidine, quinoline, tetrahydroquinoline, guanide, p-xylyl-enediamine, indole, and cyclic pentapeptide are commonly known pharmacophores as CXCR4 inhibitors (Debnath et al., 2013). The compounds **3, 6**, and **27** possess relatively different structural architectures that do not know resemble with these moieties. This suggests that the discovery of **3, 6**, and **27** as anit-HIV drugs could provide and new platform with a unique set of compounds that do not resemble with already known CXCR4 inhibitors. Among potent CCR5 inhibitors, maraviroc has 8-azabicyclo[3.2.1]octane and triazole residues, vicriviroc has piprazine, trifluoromethyl, and pyrimidine residues, aplaviroc contain 1,4,9-triazaspiro[5.5]undecane and cenicriviroc is composed of biphenyl with fused tetrahydroazocine and imidazole (Maeda et al., 2012). The only similarity of the compounds reported in this study was found in the form of piprazine in **6**, which resembles vicriviroc.

Additionally, it is worth mentioning that the high selectivity of compound **27** towards CCR5 could serve as a promising starting point for further optimization towards novel and more potent CCR5 antagonists. Moreover, it is notable that among the 27 screened compounds, 13 of them displayed antiviral activity against HIV-1 in low to medium micromolar range, which indicates an enrichment rate of

approximately 48.14% (at 100 μM cutoff). Hence, this systematic study focuses on an additional argument emphasizing the advantages of virtual screening for discovering new drug candidates.

5. Conclusion

The study outlines the identification of new selective CCR5 and CXCR4 antagonists, as well as the discovery of a dual CCR5/CXCR4 antagonist. The important pitfalls that must be addressed in virtual screening efforts against chemokine receptors is defining an effective scoring method using electrostatic surface potentials towards hit selection and prioritization. The pipeline of receptor- and ligand-based virtual screening, used in this study, proved as a promising tool to find antagonists for the selected targets. The results were validated through specific Ca^{2+} GPCR signaling assays and via an anti-HIV-1 replication assay using CXCR4- and CCR5-tropicNL4.3 and BaL strains. Quantitative structure activity relationship studies and synthesis of related derivatives could serve as a future direction for anti-HIV discovery. Moreover, the provided information can open up new possibilities for the computer-aided discovery and design of novel chemokine receptor ligands with comparable modes of action.

Author contributions

Muhammad Usman Mirza: performed in silico analysis, literature review, lead selection and manuscript writing Atefeh Saadabadi and Michiel Vanmeert: in silico analysis Outi M. H. Salo-Ahen: supervised Schrodinger suite analysis Iskandar Abdullah: literature review and data analysis Sandra Claes and Steven De Jonghe: performed antiviral assay Dominique Schols: supervised antiviral assay Sarfraz Ahmad: lead selection, literature and data analysis and manuscript writing Matheus Froeyen: conceived idea, designed the experiments and supervised project. All the authors approved the final manuscript.

Supplementary materials

Supplementary material associated with this article can be found, in the online version, at doi:10.1016/j.ejps.2020.105537.

References

Abreu, C.M., Price, S.L., Shirk, E.N., Cunha, R.D., Pianowski, L.F., Clements, J.E., Tanuri, A., Gama, L., 2014. Dual role of novel ingenol derivatives from Euphorbia tirucalli in HIV replication: inhibition of de novo infection and activation of viral LTR. PLoS One 9.

Allewijn, F.T.N., 1968. The distribution of cinnarizine and its metabolites in the rat. Life Sci. 7, 989–994.

Barber, J.H., Reuter, C.A., Jageneau, A.H., Loots, W., 1980. Intermittent claudication: a controlled study in parallel time of the short-term and long-term effects of cinnarizine. Pharmatherapeutica 2, 401.

Batool, M., Ahmad, B., Choi, S., 2019. A structure-based drug discovery paradigm. Int. J. Mol. Sci. 20, 2783.

Bennion, B.J., Be, N.A., McNerney, M.W., Lao, V., Carlson, E.M., Valdez, C.A., Malfatti, M.A., Enright, H.A., Nguyen, T.H., Lightstone, F.C., 2017. Predicting a drug's membrane permeability: A computational model validated with in vitro permeability assay data. J. Phys. Chem. B 121, 5228–5237.

Brücke, T., Wöber, C.H., Podreka, I., Wöber-Bingöl, C., Asenbaum, S., Aull, S., Wenger, S., Ilieva, D., van der Meer, C.H., Wessely, P., 1995. D2 receptor blockade by flunarizine and cinnarizine explains extrapyramidal side effects. A SPECT study. J. Cerebral Blood Flow Metabolism 15, 513–518.

Cardozo, T., Kimura, T., Philpott, S., Weiser, B., Burger, H., Zolla-Pazner, S., 2007. Structural basis for coreceptor selectivity by the HIV type 1 V3 loop. AIDS Res. Hum. Retroviruses 23, 415–426.

Case, D.A., Ben-Shalom, I.Y., Brozell, S.R., Cerutti, D.S., Cheatham Iii, T.E., Cruzeiro, V.W.D., Darden, T.A., Duke, R.E., Ghoreishi, D., Gilson, M.K., 2018. In: Proceedings of the AMBER. University of California, San Francisco.

Castaneda-Hernandez, G., Vargas-Alvarado, Y., Aguirre, F., Flores-Murrieta, F.J., 1993. Pharmacokinetics of cinnarizine after single and multiple dosing in healthy volunteers. Arzneimittel-Forschung/Drug Research 539–542.

Castonguay, L.A., Weng, Y., Adolfsen, W., Di Salvo, J., Kilburn, R., Caldwell, C.G., Daugherty, B.L., Finke, P.E., Hale, J.J., Lynch, C.L., 2003. Binding of 2-aryl-4-(piperidin-1-yl) butanamines and 1, 3, 4-trisubstituted pyrrolidines to human CCR5: a molecular modeling-guided mutagenesis study of the binding pocket. Biochemistry 42, 1544–1550.

Cazzola, M., Testi, R., Matera, M.G., 2002. Clinical pharmacokinetics of salmeterol. Clin. Pharmacokinet. 41, 19–30.

Chen, W., Zhan, P., De Clercq, E., Liu, X., 2012. Recent progress in small molecule CCR5 antagonists as potential HIV-1 entry inhibitors. Current Pharm. Des. 18, 100–112.

Chen, B., 2019. Molecular mechanism of HIV-1 entry. Trends Microbiol. 27, 878–891.

Cheng, L.S., Amaro, R.E., Xu, D., Li, W.W., Arzberger, P.W., McCammon, J.A., 2008. Ensemble-based virtual screening reveals potential novel antiviral compounds for avian influenza neuraminidase. J. Med. Chem. 51, 3878–3894.

Chien, H.-C., Chan, P.-C., Tu, C.-C., Day, Y.-J., Hung, L.-M., Juan, C.-C., Tian, Y.-F., Hsieh, P.-S., 2018. Importance of PLC-dependent PI3K/AKT and AMPK signaling in RANTES/CCR5 mediated macrophage chemotaxis. Chin. J. Physiol. 266–279.

Cobucci, R.N.O., Lima, P.H., de Souza, P.C., Costa, V.V., de Mesquita Cornetta, M.d.C., Fernandes, J.V., Gonçalves, A.K., 2015. Assessing the impact of HAART on the incidence of defining and non-defining AIDS cancers among patients with HIV/AIDS: a systematic review. J. Infect Public Heal. 8, 1–10.

Cox, B.D., Prosser, A.R., Sun, Y., Li, Z., Lee, S., Huang, M.B., Bond, V.C., Snyder, J.P., Krystal, M., Wilson, L.J., 2015. Pyrazolo-piperidines exhibit dual inhibition of CCR5/CXCR4 HIV entry and reverse transcriptase. ACS Med. Chem. Lett. 6, 753–757.

De Clercq, E., 2009. The AMD3100 story: the path to the discovery of a stem cell mobilizer (Mozobil). Bioch. Pharmacol. 77, 1655–1664.

De Jong, J.J., De Ronde, A., Keulen, W., Tersmette, M., Goudsmit, J., 1992. Minimal requirements for the human immunodeficiency virus type 1 V3 domain to support the syncytium-inducing phenotype: analysis by single amino acid substitution. J. Virol. 66, 6777–6780.

Debnath, B., Xu, S., Grande, F., Garofalo, A., Neamati, N., 2013. Small molecule inhibitors of CXCR4. Theranostics 3, 47.

Dixon, S.L., Smondyrev, A.M., Knoll, E.H., Rao, S.N., Shaw, D.E., Friesner, R.A., 2006. PHASE: a new engine for pharmacophore perception, 3D QSAR model development, and 3D database screening: 1. Methodology and preliminary results. J. Comput. Aided Mol. Des. 20, 647–671.

Dixon, S.L., Smondyrev, A.M., Rao, S.N., 2006. PHASE: a novel approach to pharmacophore modeling and 3D database searching. Chem. Biol. Drug Des. 67, 370–372.

Dorr, P., Westby, M., Dobbs, S., Griffin, P., Irvine, B., Macartney, M., Mori, J., Rickett, G., Smith-Burchnell, C., Napier, C., 2005. Maraviroc (UK-427,857), a potent, orally bioavailable, and selective small-molecule inhibitor of chemokine receptor CCR5 with broad-spectrum anti-human immunodeficiency virus type 1 activity. Antimicrobial Agents Chemother. 49, 4721–4732.

Dragic, T., Litwin, V., Allaway, G.P., Martin, S.R., Huang, Y., Nagashima, K.A., Cayanan, C., Maddon, P.J., Koup, R.A., Moore, J.P., 1996. HIV-1 entry into CD4+ cells is mediated by the chemokine receptor CC-CKR-5. Nature 381, 667–673.

Dragic, T., Trkola, A., Thompson, D.A.D., Cormier, E.G., Kajumo, F.A., Maxwell, E., Lin, S.W., Ying, W., Smith, S.O., Sakmar, T.P., 2000. A binding pocket for a small molecule inhibitor of HIV-1 entry within the transmembrane helices of CCR5. Proc. Natl. Acad. Sci. 97, 5639–5644.

Fouchier, R.A., Groenink, M., Kootstra, N.A., Tersmette, M., Huisman, H.G., Miedema, F., Schuitemaker, H., 1992. Phenotype-associated sequence variation in the third variable domain of the human immunodeficiency virus type 1 gp120 molecule. J. Virol. 66, 3183–3187.

Garcia-Perez, J., Rueda, P., Alcami, J., Rognan, D., Arenzana-Seisdedos, F., Lagane, B., Kellenberger, E., 2011. Allosteric model of maraviroc binding to CC chemokine receptor 5 (CCR5). J. Biol. Chem. 286, 33409–33421.

Giroud, C., Marin, M., Hammonds, J., Spearman, P., Melikyan, G.B., 2015. P2X1 receptor antagonists inhibit HIV-1 fusion by blocking virus-coreceptor interactions. J. Virol. 89, 9368–9382.

Govaerts, C., Bondue, A., Springael, J.-Y., Olivella, M., Deupi, X., Le Poul, E., Wodak, S.J., Parmentier, M., Pardo, L., Blanpain, C., 2003. Activation of CCR5 by chemokines involves an aromatic cluster between transmembrane helices 2 and 3. J. Biol. Chem. 278, 1892–1903.

Grande, F., Garofalo, A., Neamati, N., 2008. Small molecules anti-HIV therapeutics targeting CXCR4. Current Pharma. Des. 14, 385–404.

Grande, F., Occhiuzzi, M.A., Rizzuti, B., Ioele, G., De Luca, M., Tucci, P., Svicher, V., Aquaro, S., Garofalo, A., 2019. CCR5/CXCR4 dual antagonism for the improvement of HIV infection therapy. Molecules 24, 550.

Halgren, T.A., Murphy, R.B., Friesner, R.A., Beard, H.S., Frye, L.L., Pollard, W.T., Banks, J.L., 2004. Glide: a new approach for rapid, accurate docking and scoring. 2. Enrichment factors in database screening. J. Med. Chem. 47, 1750–1759.

Hatse, S., Princen, K., Gerlach, L.-O., Bridger, G., Henson, G., De Clercq, E., Schwartz, T.W., Schols, D., 2001. Mutation of Asp171 and Asp262 of the chemokine receptor CXCR4 impairs its coreceptor function for human immunodeficiency virus-1 entry and abrogates the antagonistic activity of AMD3100. Mol. Pharmacol. 60, 164–173.

Heredia, J.D., Park, J., Brubaker, R.J., Szymanski, S.K., Gill, K.S., Procko, E., 2018. Mapping interaction sites on human chemokine receptors by deep mutational scanning. J. Immunol. 200, 3825–3839.

Hill, R.L.R., 2002. The bioavailability of mupirocin in nasal secretions in vitro. J. Clin. Pathol. 55, 233–235.

Horuk, R., 2009. Promiscuous drugs as therapeutics for chemokine receptors. Expert Rev. Mol. Med. 11, E1.

Hou, T., Wang, J., Li, Y., Wang, W., 2011. Assessing the performance of the MM/PBSA and MM/GBSA methods. 1. The accuracy of binding free energy calculations based on molecular dynamics simulations. J. Chem. Inf. Model. 51, 69–82.

Hubin, T.J., Archibald, S.J., Won, P., Birdsong, O.C., Epley, B.M., Klassen, S.L., Schols, D., 2013. Synthesis and evaluation of transition metal complex dual CXCR4/CCR5 antagonists. In: Proceedings of the National Spring Meeting of the American Chemical Society. American Chemical Society.

Ikram, N., Mirza, M.U., Vanmeert, M., Froeyen, M., Salo-Ahen, O.M.H., Tahir, M., Qazi,

A., Ahmad, S., 2019. Inhibition of oncogenic kinases: an in vitro validated computational approach identified potential multi-target anticancer compounds. Biomolecules 9, 124.
Jacobson, M.P., Pincus, D.L., Rapp, C.S., Day, T.J.F., Honig, B., Shaw, D.E., Friesner, R.A., 2004. A hierarchical approach to all-atom protein loop prediction. Proteins Struct. Funct. Bioinf. 55, 351–367.
Kudo, E., Taura, M., Matsuda, K., Shimamoto, M., Kariya, R., Goto, H., Hattori, S., Kimura, S., Okada, S., 2013. Inhibition of HIV-1 replication by a tricyclic coumarin GUT-70 in acutely and chronically infected cells. Bioorganic Med. Chem. Lett. 23, 606–609.
Li, J., Abel, R., Zhu, K., Cao, Y., Zhao, S., Friesner, R.A., 2011. The VSGB 2.0 model: a next generation energy model for high resolution protein structure modeling. Proteins Struct. Funct. Bioinf. 79, 2794–2812.
Loetscher, M., Geiser, T., O'Reilly, T., Zwahlen, R., Baggiolini, M., Moser, B., 1994. Cloning of a human seven-transmembrane domain receptor, LESTR, that is highly expressed in leukocytes. J. Biol. Chem. 269, 232–237.
Luo, M., Groaz, E., Andrei, G., Snoeck, R., Kalkeri, R., Ptak, R.G., Hartman, T., Buckheit Jr, R.W., Schols, D., De Jonghe, S., 2017. Expanding the antiviral Spectrum of 3-Fluoro-2-(phosphonomethoxy) propyl acyclic nucleoside phosphonates: Diamyl aspartate Amidate prodrugs. J. Med. Chem. 60, 6220–6238.
Maeda, K., Das, D., Nakata, H., Mitsuya, H., inhibitors, CCR5, 2012. emergence, success, and challenges. Expert Opin. Emerg. Drugs 17, 135–145.
Maier, J.A., Martinez, C., Kasavajhala, K., Wickstrom, L., Hauser, K.E., Simmerling, C., 2015. ff14SB: improving the accuracy of protein side chain and backbone parameters from ff99SB. J. Chem. Theory Comput. 11, 3696–3713.
Manara, A., Hantson, P., Vanpee, D., Thys, F., 2012. Lactic acidosis following intentional overdose by inhalation of salmeterol and fluticasone. Can. J. Emerg. Med. 14, 378–381.
Medigeshi, G.R., Kumar, R., Dhamija, E., Agrawal, T., Kar, M., 2016. N-desmethylclozapine, fluoxetine, and salmeterol inhibit postentry stages of the dengue virus life cycle. Antimicrob. Agents Chemother. 60, 6709–6718.
Mirza, M.U., Froeyen, M., 2020. Structural elucidation of SARS-CoV-2 vital proteins: Computational methods reveal potential drug candidates against main protease, Nsp12 polymerase and Nsp13 helicase. J. Pharm. Anal.
Mirza, M.U., Vanmeert, M., Ali, A., Iman, K., Froeyen, M., Idrees, M., 2019. Perspectives towards antiviral drug discovery against Ebola virus. J. Med. Virol. 91, 2029–2048.
Mirza, M.U., Vanmeert, M., Froeyen, M., Ali, A., Rafique, S., Idrees, M., 2019. In silico structural elucidation of RNA-dependent RNA polymerase towards the identification of potential Crimean-Congo Hemorrhagic Fever Virus inhibitors. Sci. Rep. 9, 1–18.
Neves, M.A.C., Simões, S., e Melo, M.L.S., 2010. Ligand-guided optimization of CXCR4 homology models for virtual screening using a multiple chemotype approach. J. Comput. Aided Mol. Des. 24, 1023–1033.
Nguyen, T.T.H., Ryu, H.-J., Lee, S.-H., Hwang, S., Breton, V., Rhee, J.H., Kim, D., 2011. Virtual screening identification of novel severe acute respiratory syndrome 3C-like protease inhibitors and in vitro confirmation. Bioorg. Med. Chem. Lett. 21, 3088–3091.
A.N. Nicholson, B.M. Stone, C. Turner, S.L. Mills, Central effects of cinnarizine: restricted use in aircrew, aviation, space, and environmental medicine, 73 (2002) 570-574.
Nishikawa, M., Takashima, K., Nishi, T., Furuta, R.A., Kanzaki, N., Yamamoto, Y., Fujisawa, J.-i., 2005. Analysis of binding sites for the new small-molecule CCR5 antagonist TAK-220 on human CCR5. Antimicrob. Agents Chemother. 49, 4708–4715.
Oliva-Moreno, J., Trapero-Bertran, M., 2018. Economic impact of HIV in the highly active antiretroviral therapy era—reflections looking forward. AIDS Rev. 20, 226–235.
Oppermann, M., 2004. Chemokine receptor CCR5: insights into structure, function, and regulation. Cell. Signal. 16, 1201–1210.
Pappa, K.A., 1990. The clinical development of mupirocin. J. Am. Acad. Dermatol. 22, 873–879.
Parenti, M.A., Hatfield, S.M., Leyden, J.J., 1987. Mupirocin: a topical antibiotic with a unique structure and mechanism of action. Clin. Pharm. 6, 761–770.
Peng, Y., McCorvy, J.D., Harpsøe, K., Lansu, K., Yuan, S., Popov, P., Qu, L., Pu, M., Che, T., Nikolajsen, L.F., 2018. 5-HT2C receptor structures reveal the structural basis of GPCR polypharmacology. Cell 172, 719–730.
Price, D.A., Armour, D., de Groot, M., Leishman, D., Napier, C., Perros, M., Stammen, B.L., Wood, A., 2006. Overcoming HERG affinity in the discovery of the CCR5 antagonist maraviroc. Bioorg. Med. Chem. Lett. 16, 4633–4637.
Princen, K., Hatse, S., Vermeire, K., Aquaro, S., De Clercq, E., Gerlach, L.-O., Rosenkilde, M., Schwartz, T.W., Skerlj, R., Bridger, G., 2004. Inhibition of human immunodeficiency virus replication by a dual CCR5/CXCR4 antagonist. J. Virol. 78, 12996–13006.
Roe, D.R., Cheatham Iii, T.E., 2013. PTRAJ and CPPTRAJ: software for processing and analysis of molecular dynamics trajectory data. J. Chem. Theory Comput. 9, 3084–3095.
Roos, K., Wu, C., Damm, W., Reboul, M., Stevenson, J.M., Lu, C., Dahlgren, M.K., Mondal, S., Chen, W., Wang, L., 2019. OPLS3e: Extending force field coverage for drug-like small molecules. J. Chem. Theory Comput. 15, 1863–1874.
Rosenthal, R.R., Busse, W.W., Kemp, J.P., Baker, J.W., Kalberg, C., Emmett, A., Rickard, K.A., 1999. Effect of long-term salmeterol therapy compared with as-needed albuterol use on airway hyperresponsiveness. Chest 116, 595–602.
Santos, F., Nunes, D.A.d.F., Lima, W.G., Davyt, D., Santos, L.L., Taranto, A.G., Maria Siqueira Ferreira, J., 2019. Identification of Zika virus NS2B-NS3 protease inhibitors by structure-based virtual screening and drug repurposing approaches. J. Chem. Inf. Model. 60, 731–737.
Sastry, G.M., Adzhigirey, M., Day, T., Annabhimoju, R., Sherman, W., 2013. Protein and ligand preparation: parameters, protocols, and influence on virtual screening enrichments. J. Comput. Aided Mol. Des. 27, 221–234.
Scarlatti, G., Tresoldi, E., Björndal, Å., Fredriksson, R., Colognesi, C., Deng, H.K., Malnati, M.S., Plebani, A., Siccardi, A.G., Littman, D.R., 1997. In vivo evolution of HIV-1 co-receptor usage and sensitivity to chemokine-mediated suppression. Nat. Med. 3, 1259–1265.
Scholten, D.J., Canals, M., Maussang, D., Roumen, L., Smit, M.J., Wijtmans, M., De Graaf, C., Vischer, H.F., Leurs, R., 2012. Pharmacological modulation of chemokine receptor function. Br. J. Pharmacol. 165, 1617–1643.
Seibert, C., Sakmar, T.P., 2004. Small-molecule antagonists of CCR5 and CXCR4: a promising new class of anti-HIV-1 drugs. Curr. Pharm. Des. 10, 2041–2062.
Shaikh, F., Zhao, Y., Alvarez, L., Iliopoulou, M., Lohans, C., Schofield, C.J., Padilla-Parra, S., Siu, S.W., Fry, E.E., Ren, J., 2019. Structure-based in silico screening identifies a potent ebolavirus inhibitor from a traditional chinese medicine library. J. Med. Chem. 62, 2928–2937.
Shepherd, A.J., Loo, L., Mohapatra, D.P., 2013. Chemokine co-receptor CCR5/CXCR4-dependent modulation of Kv2. 1 channel confers acute neuroprotection to HIV-1 glycoprotein gp120 exposure,. PLoS One 8, e7669.
Shimizu, N., Haraguchi, Y., Takeuchi, Y., Soda, Y., Kanbe, K., Hoshino, H., 1999. Changes in and discrepancies between cell tropisms and coreceptor uses of human immunodeficiency virus type 1 induced by single point mutations at the V3 tip of the env protein. Virology 259, 324–333.
Singh, I.P., Chauthe, S.K., 2011. Small molecule HIV entry inhibitors: Part II. Attachment and fusion inhibitors: 2004–2010. Expert Opin. Therapeutic Patents 21, 399–416.
O. Slater, M.J.E.o.o.d.d. Kontoyianni, The compromise of virtual screening and its impact on drug discovery, 14 (2019) 619-637.
Smith, N., Pietrancosta, N., Davidson, S., Dutrieux, J., Chauveau, L., Cutolo, P., Dy, M., Scott-Algara, D., Manoury, B., Zirafi, O., 2017. Natural amines inhibit activation of human plasmacytoid dendritic cells through CXCR4 engagement. Nat. Commun. 8, 1–13.
Srivastava, H.K., Sastry, G.N., 2012. Molecular dynamics investigation on a series of HIV protease inhibitors: assessing the performance of MM-PBSA and MM-GBSA approaches. J. Chem. Inf. Model. 52, 3088–3098.
Tahirovic, Y.A., Pelly, S., Jecs, E., Miller, E.J., Sharma, S.K., Liotta, D.C., Wilson, L.J., 2020. Small molecule and peptide-based CXCR4 modulators as therapeutic agents. A patent review for the period from 2010 to 2018. Expert Opin. Therapeutic Patents 30, 87–101.
J.J. Tan, W. Zu Chen, C.X.J.J.o.M.S.T. Wang, Investigating interactions between HIV-1 gp41 and inhibitors by molecular dynamics simulation and MM–PBSA/GBSA calculations, 766 (2006) 77-82.
Tan, Q., Zhu, Y., Li, J., Chen, Z., Han, G.W., Kufareva, I., Li, T., Ma, L., Fenalti, G., Li, J., 2013. Structure of the CCR5 chemokine receptor–HIV entry inhibitor maraviroc complex. Science 341, 1387–1390.
Tan, S., Yang, B., Liu, J., Xun, T., Liu, Y., Zhou, X., Penicillixanthone, A, 2019. a marine-derived dual-coreceptor antagonist as anti-HIV-1 agent. Nat. Product Res. 33, 1467–1471.
Taylor, C.A., Miller Iii, B.R., Parish, C.A., 2017. Design and computational support for the binding stability of a new CCR5/CXCR4 dual tropic inhibitor: computational design of a CCR5/CXCR4 drug. J. Mol. Graph. Model. 75, 71–79.
Teive, H.A.G., Troiano, A.R., Germiniani, F.M.B., Werneck, L.C., 2004. Flunarizine and cinnarizine-induced parkinsonism: a historical and clinical analysis. Parkinsonism Relat. Disord. 10, 243–245.
Tsamis, F., Gavrilov, S., Kajumo, F., Seibert, C., Kuhmann, S., Ketas, T., Trkola, A., Palani, A., Clader, J.W., Tagat, J.R., 2003. Analysis of the mechanism by which the small-molecule CCR5 antagonists SCH-351125 and SCH-350581 inhibit human immunodeficiency virus type 1 entry. J. Virol. 77, 5201–5208.
F. Tuzer, N. Madani, K. Kamanna, I. Zentner, J. LaLonde, A. Holmes, E. Upton, S. Rajagopal, K. McFadden, M.J.P.S. Contarino, Function, , Bioinformatics, HIV-1 ENV gp120 structural determinants for peptide triazole dual receptor site antagonism, 81 (2013) 271-290.
Van Hout, A., D'huys, T., Oeyen, M., Schols, D., Van Loy, T., 2017. Comparison of cell-based assays for the identification and evaluation of competitive CXCR4 inhibitors. PLoS One 12, e0176057.
Wilder-Smith, C.H., Schimke, J., Osterwalder, B., Senn, H.J., 1991. Cinnarizine for prevention of nausea and vomiting during platin chemotherapy. Acta Oncol. (Madr) 30, 731–734.
Wu, B., Chien, E.Y.T., Mol, C.D., Fenalti, G., Liu, W., Katritch, V., Abagyan, R., Brooun, A., Wells, P., Bi, F.C., 2010. Structures of the CXCR4 chemokine GPCR with small-molecule and cyclic peptide antagonists. Science 330, 1066–1071.
Yuan, S., Chan, J.F.-W., den-Haan, H., Chik, K.K.-H., Zhang, A.J., Chan, C.C.-S., Poon, V.K.-M., Yip, C.C.-Y., Mak, W.W.-N., Zhu, Z., 2017. Structure-based discovery of clinically approved drugs as Zika virus NS2B-NS3 protease inhibitors that potently inhibit Zika virus infection in vitro and in vivo. Antiviral Res. 145, 33–43.
Zhou, Z., Khaliq, M., Suk, J.-E., Patkar, C., Li, L., Kuhn, R.J., Post, C.B., 2008. Antiviral compounds discovered by virtual screening of small− molecule libraries against dengue virus E protein. ACS Chem. Biol. 3, 765–775.
Zhukovsky, M.A., Lee, P.H., Ott, A., Helms, V., 2013. Putative cholesterol-binding sites in human immunodeficiency virus (HIV) coreceptors CXCR4 and CCR5. Proteins Struct. Funct. Bioinf. 81, 555–567.